
Model Density Approach to the Kohn–Sham Problem: Efficient Extension of the Density Fitting Technique

UWE BIRKENHEUER,^{1*} ALEKSEI B. GORDIENKO,^{1†}
VLADIMIR A. NASLUZOV,^{1,2} MONIKA K. FUCHS-ROHR,^{1‡}
NOTKER RÖSCH¹

¹*Department Chemie, Technische Universität München, 85747 Garching, Germany*

²*Institute of Chemistry and Chemical Technology, Russian Academy of Sciences, Krasnoyarsk, Russian Federation*

Received 3 August 2004; accepted 25 October 2004

Published online 12 January 2005 in Wiley InterScience (www.interscience.wiley.com).

DOI 10.1002/qua.20447

ABSTRACT: We present a novel procedure for treating the exchange–correlation contributions in the Kohn–Sham procedure. The approach proposed is fully variational and closely related to the so-called “fitting functions” method for the Coulomb Hartree problem; in fact, the method consistently uses this auxiliary representation of the electron density to determine the exchange–correlation contributions. The exchange–correlation potential and its matrix elements in a basis set of localized (atomic) orbitals can be evaluated by reusing the three-center Coulomb integrals involving fitting functions, while the computational cost of the remaining numerical integration is significantly reduced and scales only linearly with the size of the auxiliary basis. We tested the approach extensively for a large set of atoms and small molecules as well as for transition-metal carbonyls and clusters, by comparing total energies, atomization energies, structure parameters, and vibrational frequencies at the local density approximation and generalized gradient approximation levels of theory. The method requires a sufficiently flexible auxiliary basis set. We propose a minimal extension of the conventional auxiliary basis set, which yields essentially the same accuracy for the quantities just mentioned as the standard approach. The new method allows one to achieve substantial savings compared with a fully numerical integration of the exchange–correlation contributions. © 2005 Wiley Periodicals, Inc. *Int J Quantum Chem* 102: 743–761, 2005

Key words: density functional; variationally consistent fitting; exchange–correlation potential

Correspondence to: U. Birkenheuer; e-mail: birken@mpipks-dresden.mpg.de or N. Rösch; e-mail: roesch@ch.tum.de

*Present address: Max-Planck Institut für Physik Komplexer Systeme, 01187 Dresden, Germany.

†Permanent address: Department of Theoretical Physics, Kemerovo State University, 650043 Kemerovo, Russian Federation.

‡Present address: European Patent Office, Munich, Germany.

Contract grant sponsor: Volkswagen Foundation.

Contract grant number: I/73653.

Contract grant sponsor: INTAS/RFBR.

Contract grant number: IR-97-1071/RFBR 97-03-71057.

Contract grant sponsor: Fonds der Chemischen Industrie.

Introduction

Density functional theory (DFT) [1, 2] is now recognized as a very powerful tool in physics and chemistry that allows one to address a wide range of problems related to the electronic structure of molecules, clusters, surfaces, and solids [3, 4]. A very attractive feature of the Kohn–Sham (KS) approach to DFT is the approximate treatment of electron correlation in an effective one-electron picture. With modern approximations of the exchange–correlation (xc) functional, the KS approach achieves an accuracy that often rivals post–Hartree–Fock correlation methods, but at a computational effort that is only somewhat larger than that of a Hartree–Fock (HF) self-consistent field (SCF) calculation [5–15]. Implementations that make judicious use of fitting (or resolution of identity) techniques to represent the classical Coulomb (Hartree) part of the electron–electron interaction achieve favorable performance in molecular density functional (DF) calculations [16–19]. By introducing auxiliary or fitting functions to represent the total (spin) density, one avoids the costly evaluation of four-center integrals in the Roothaan approach to the KS problem [20–22]. This approximation, first suggested in conventional quantum chemistry [23], was already used in early implementations of the Roothaan approach to the KS method [24]. With the fitting strategy, the formal scaling of the Coulomb problem is reduced from $O(N^4)$ to $O(N^3)$, N quantifying the size of the basis sets. Note that the use of a variational fitting procedure, for example, the minimization of the Coulomb self-interaction of the distribution characterizing the fitting [25], permits a systematic improvement of the auxiliary charge density representation, similar to the Roothaan representation of the molecular orbitals (MOs) employed in the KS approach.

On the other hand, the advantage of purely analytical integral evaluation inherent to the Roothaan approach to HF-based methods cannot be easily transferred to KS calculations, because of the complicated algebraic form of the xc functional and the corresponding contribution to the one-electron potential. Even in the simplest form of Slater’s $X\alpha$ approximation [22, 26] the xc potential and energy density consist of terms that comprise fractional powers of the electron density. Therefore, from the very beginning [24], most implementations of the KS approach involved numerical integration procedures on atom-centered grids. By now, techniques

for constructing efficient integration grids for molecular calculations are well developed [27–33]; they even permit a systematic improvement of the accuracy of the integration. Still, the finite precision of the numerical integration procedure restricts highly accurate DF applications at reasonable computational effort to relatively small systems. Attempts to reduce the numerical noise and, in particular, to remove the lack of rotational invariance [34, 35] with finer integration grids render highly accurate KS calculations relatively time-consuming. Hence, since the early applications of the Roothaan technique to the molecular KS problem [36], quite a few procedures have been developed to represent the xc terms in such a way that one is able to regain the advantage of fully analytical integral evaluation [16, 37–43].

In this work, we present the model density approach (MDA), which extends the variation procedure of the Hartree term (charge density fitting) to the xc functional. This method, suggested some time ago [44], significantly reduces the numerical effort to evaluate the xc contributions. Just as the well-known treatment of the Hartree term is based on an approximate expression of the Hartree Coulomb energy and the corresponding potential [25], the MDA employs consistent approximations to the xc energy and the corresponding potential. Aiming, in particular, at a computational scheme that is well-suited for complex systems, accurate nuclear forces (and other first derivatives of the total energy) are an important asset that entails efficient structure optimizations and dynamic simulations. Yet forces that are fully consistent with the underlying energy potential surface can be obtained only if all approximations introduced to evaluate both the xc contributions to the total energy and the potential are carried out in proper accordance with one another, an issue that is often neglected in approximative implementations of DFT.

The paper is organized as follows. In the next section, we briefly review the Coulomb fitting approach, which we then extend to the MDA formalism that allows an analytical evaluation of the xc terms. In the third section, we present and analyze a series of test calculations for atoms, polyatomic molecules, and clusters, performed both with a local density approximation (LDA) and a generalized-gradient approximation (GGA), and we discuss the computational performance of the MDA and compare it with a conventional numeric treatment as implemented in the code PARAGAUSS [45,

46]. For some details of the implementation, the reader is referred to the Appendix.

Model Density Approach

VARIATIONAL CONSISTENCY

The model density approach is guided by the idea to simplify the evaluation of a given local (or quasiloc) xc functional $E_{xc}[\rho]$ and the associated xc potential $V_{xc}[\rho]$, by switching to approximate expressions $\tilde{E}_{xc}[\rho]$ and $\tilde{V}_{xc}[\rho]$ for these energy and potential contributions, which are computationally more convenient. Of course, the same strategy can also be applied to the Coulomb energy and potential. Doing so, the total DFT energy within the KS approach becomes

$$E_{\text{tot}} = \sum_n f_n \langle \psi_n | T | \psi_n \rangle + \langle \rho | V_{\text{ext}} \rangle + \tilde{E}_{\text{ee}} + E_{\text{nnv}} \quad (1)$$

with $\rho = \sum_n f_n |\psi_n|^2$ and $\psi_n = \sum_\nu \chi_\nu c_{\nu n}$; χ_ν is an MO basis function and $c_{\nu n}$ the corresponding coefficient of KS orbital ψ_n with energy ε_n and occupation number f_n . Then the KS equation reads

$$\sum_\mu \langle \chi_\nu | T + V_{\text{ext}} + \tilde{V}_{\text{ee}} | \chi_\mu \rangle c_{\mu n} = \varepsilon_n \sum_\mu \langle \chi_\nu | \chi_\mu \rangle c_{\mu n}. \quad (2)$$

Here, \tilde{E}_{ee} and \tilde{V}_{ee} comprise both approximate Coulomb and approximate xc contributions. The first derivative of the total energy with respect to some parameter λ , for example, a nuclear position or the strength of a perturbative external field, is

$$\begin{aligned} \frac{dE_{\text{tot}}}{d\lambda} = & \left\langle \rho \left| \frac{dV_{\text{ext}}}{d\lambda} \right. \right\rangle + \frac{dE_{\text{nuc}}}{d\lambda} + \sum_n \varepsilon_n \frac{df_n}{d\lambda} \\ & + \sum_n 2f_n \left\langle \sum_\nu \frac{d\chi_\nu}{d\lambda} c_{\nu n} \left| T + V_{\text{ext}} + \tilde{V}_{\text{ee}} - \varepsilon_n \right| \psi_n \right\rangle \\ & + \frac{\partial \tilde{E}_{\text{ee}}}{\partial \lambda} + \left\langle \frac{d\rho}{d\lambda} \left| \frac{\delta \tilde{E}_{\text{ee}}}{\delta \rho} - \tilde{V}_{\text{ee}} \right. \right\rangle. \quad (3) \end{aligned}$$

The first line contains the Hellmann–Feynman forces [47, 48] and a “thermal” correction, which arises if level broadening is used and the fractional occupation numbers depend on the parameter λ [16]; this term can be avoided if the total energy functional is replaced by a free energy functional [49–51]. For simplicity, we consider only the case of

fixed occupation numbers in the following. The second line of Eq. (3) gives the Pulay corrections [52], which derive from the incompleteness of the MO basis set with respect to changes of λ . Finally, the third line shows the contributions associated with the approximate two-electron terms of the total energy and the KS Hamiltonian. The partial derivative in these latter terms indicates that only the explicit λ dependence of the functional $\tilde{E}_{\text{ee}}[\rho]$ — and not the one mediated through the (implicit) λ dependence of the charge density ρ — is to be differentiated.

The most demanding contribution to the first-order energy derivative $dE_{\text{tot}}/d\lambda$ is the last term of Eq. (3), the response of the self-consistent charge density to infinitesimal changes of the parameter λ ; to evaluate it, one has to invoke first-order orbital perturbation theory. This term can be avoided only if the approximations to the two-electron energy and the corresponding potential contribution are strictly consistent. In other words, whatever approximation is introduced in $\tilde{E}_{\text{ee}}[\rho]$, the approximation to $\tilde{V}_{\text{ee}}[\rho](r)$ must obey the condition

$$\tilde{V}_{\text{ee}}[\rho](\mathbf{r}) = \frac{\delta \tilde{E}_{\text{ee}}[\rho]}{\delta \rho(\mathbf{r})}. \quad (4)$$

CHARGE DENSITY FITTING

We first demonstrate the power of the concept of variational consistency for the Hartree part of the two-electron energy. This also allows us to introduce the charge density fitting procedure used below and to suggest some general notations. For the sake of brevity, we restrict the discussion to a closed-shell case, that is, without spin polarization; the generalization to an open-shell situation is straightforward.

We represent the electron density ρ in a set of (preferentially, but not necessarily atom-centered) fitting functions $\{\rho_k\}$ [53]:

$$\rho \approx \rho_{\text{fit}} = \sum_k a_k \rho_k. \quad (5)$$

The fitting coefficients a_k can then be determined by minimizing the Coulomb self-interaction functional [25]:

$$\frac{1}{2} [\rho_{\text{fit}} - \rho | \rho_{\text{fit}} - \rho] = \min,$$

$$[\rho|\rho'] = \iint \frac{\rho(\mathbf{r})\rho'(\mathbf{r}')}{|\mathbf{r}-\mathbf{r}'|} d^3\mathbf{r}d^3\mathbf{r}' \quad (6)$$

under the constraint of charge conservation, that is,

$$Q[\rho_{\text{fit}}] = Q[\rho] \equiv N, \quad (7)$$

where $Q[\rho] = \int \rho(r)d^3r$; N is the total number of electrons of the system. The choice of this functional was justified elsewhere [25, 54].

Applying the stationarity condition to the functional of Eq. (6), one obtains a system of linear equations:

$$\sum_k [\rho_j|\rho_k]a_k = [\rho_j|\rho] + \alpha Q[\rho_j], \quad (8)$$

with α being the Lagrange multiplier associated with the constraint, Eq. (7). With the quantities

$$F_{jk} = [\rho_j|\rho_k], \quad A_j = [\rho_j|\rho], \quad \text{and } Q_j = Q[\rho_j], \quad (9)$$

Eqs. (7) and (8) can be rewritten,

$$\sum_k F_{jk}a_k = A_j + \alpha Q_j \quad \text{with} \quad \sum_k Q_k a_k = N, \quad (10)$$

and solved in four steps:

$$\sum_k F_{jk}\bar{a}_k = A_j, \quad (11)$$

$$\sum_k F_{jk}\bar{\bar{a}}_k = Q_j, \quad (12)$$

$$\alpha = \frac{N - \sum_k Q_k \bar{a}_k}{\sum_k Q_k \bar{\bar{a}}_k}, \quad (13)$$

$$a_k = \bar{a}_k + \alpha \bar{\bar{a}}_k. \quad (14)$$

Charge conservation can be incorporated into the fitting procedure at essentially zero cost, because Eq. (12) does not depend on the self-consistent charge density and thus can be solved once and for all.

The procedure outlined here defines a very efficient solution to the Coulomb problem of the KS formalism, because it requires only two- and three-center integrals of the form $[\rho_j|\rho_k]$ and $[\chi_\nu\chi_\mu|\rho_k]$, which can be precalculated and stored before entering the KS SCF cycle [2].

DERIVATIVES OF THE FITTED CHARGE DENSITY

Surprisingly, the above four-step procedure exhibits rather simple first-order derivatives. Differentiating directly Eqs. (11)–(14), one gets:

$$\sum_k F_{jk} \frac{d\bar{a}_k}{d\lambda} = - \sum_k \frac{dF_{jk}}{d\lambda} \bar{a}_k + \frac{dA_j}{d\lambda}, \quad (15)$$

$$\sum_k F_{jk} \frac{d\bar{\bar{a}}_k}{d\lambda} = - \sum_k \frac{dF_{jk}}{d\lambda} \bar{\bar{a}}_k, \quad (16)$$

$$\frac{d\alpha}{d\lambda} = - \frac{\sum_k Q_k \left(\frac{d\bar{a}_k}{d\lambda} + \alpha \frac{d\bar{\bar{a}}_k}{d\lambda} \right)}{\sum_k Q_k \bar{\bar{a}}_k}, \quad (17)$$

$$\frac{da_k}{d\lambda} = \frac{d\bar{a}_k}{d\lambda} + \alpha \frac{d\bar{\bar{a}}_k}{d\lambda} + \frac{d\alpha}{d\lambda} \bar{\bar{a}}_k. \quad (18)$$

In Eq. (17), we assumed the charge Q_j associated with fitting function ρ_j and the total number N of electrons to be independent of λ . These conditions hold for λ being a nuclear position, an external field parameter, or the charge density itself; on the other hand, optimization of exponents of fitting functions would require a straightforward extension of Eq. (17).

Introducing the “projected inverse” of the charge fit overlap matrix F_{jm}

$$G_{kj} = \sum_m \left[\delta_{km} - \frac{\bar{\bar{a}}_k Q_m}{\sum_l Q_l \bar{\bar{a}}_l} \right] (F^{-1})_{mj},$$

the above equations can be rewritten in compact form

$$\frac{da_k}{d\lambda} = \sum_j G_{kj} \left(\frac{dA_j}{d\lambda} - \sum_l \frac{dF_{jl}}{d\lambda} a_l \right). \quad (19)$$

The projected inverse G_{kj} is the only quantity where charge conservation, Eq. (7), shows up. If one lifts this condition, then the quantities G_{kj} reduce to the direct inverse $(F^{-1})_{kj}$ of the charge fit overlap matrix. Expanding the short-hand notations, Eq. (9), one arrives at

$$\frac{da_k}{d\lambda} = \sum_j G_{kj} \left\{ \left[\frac{d\rho_j}{d\lambda} \right] \rho - \sum_l a_l \rho_l \right\} + \left[\rho_j \left[\frac{d\rho}{d\lambda} \right] - \sum_l a_l \frac{d\rho_l}{d\lambda} \right\}. \quad (20)$$

From this expression, one can derive first-order derivatives of the fitted electron density ρ_{fit} . Starting from Eq. (5) and using the notation $\rho_k \equiv |\rho_k\rangle \equiv |\rho_k\rangle$, we obtain

$$\frac{d\rho_{\text{fit}}}{d\lambda} = \sum_{kj} |\rho_k\rangle G_{kj} \left[\rho_j \left[\frac{d\rho}{d\lambda} \right] \right] + \sum_{kj} |\rho_k\rangle G_{kj} \left[\frac{d\rho_j}{d\lambda} \right] \rho - \rho_{\text{fit}} + \left\{ 1 - \sum_{kj} |\rho_k\rangle G_{kj} |\rho_j\rangle \right\} \left[\sum_n a_n \frac{d\rho_n}{d\lambda} \right]. \quad (21)$$

The first line describes a (constrained) fitting of the λ derivative of the exact electron density; the remaining two terms show corrections due to the incompleteness of the charge fitting basis set. These latter terms vanish (as with the Pulay corrections) when each derivative $d\rho_j/d\lambda$ can precisely be expressed as a linear combination of the charge fit functions $\{\rho_k\}$.

COULOMB POTENTIAL WITHIN MDA

Following the concept of variational consistency, expressed in Eq. (4), the approximate density-dependent potential entering the KS equation has to be exactly the functional derivative of the corresponding approximate energy functional. To demonstrate this concept, consider an approximation to the Coulomb energy, which is often used in combination with the variational charge density fitting [25, 36, 54] and which is also adopted in the MDA,

$$\tilde{E}_{\text{H}}[\rho] = [\rho|\rho_{\text{fit}}] - \frac{1}{2} [\rho_{\text{fit}}|\rho_{\text{fit}}]. \quad (22)$$

This approximation is exact to first order in the density difference $\rho - \rho_{\text{fit}}$ [25]. Varying Eq. (22) with respect to the exact charge density $\rho(\mathbf{r})$ yields the associated Coulomb potential

$$\tilde{V}_{\text{H}}[\rho](\mathbf{r}) = \frac{\delta}{\delta\rho(\mathbf{r})} \left\{ [\rho|\rho_{\text{fit}}] - \frac{1}{2} [\rho_{\text{fit}}|\rho_{\text{fit}}] \right\}, \quad (23)$$

$$= V_{\text{H}}[\rho_{\text{fit}}](\mathbf{r}) - \left[\rho - \rho_{\text{fit}} \left[\frac{\delta\rho_{\text{fit}}}{\delta\rho(\mathbf{r})} \right] \right], \quad (24)$$

with $V_{\text{H}}[\rho](\mathbf{r}) = \int \rho(\mathbf{r}')/|\mathbf{r} - \mathbf{r}'|d^3\mathbf{r}'$. Let $\lambda \rightarrow \rho(\mathbf{r})$, then the second term of Eq. (23) can be calculated with the generic first-order derivative of the fitted charge density, Eq. (21). Taking advantage of $\delta\rho_k/\delta\rho = 0$, the required functional derivative of ρ_{fit} is

$$\frac{\delta\rho_{\text{fit}}(\mathbf{s})}{\delta\rho(\mathbf{r})} = \sum_{kj} \rho_k(\mathbf{s}) G_{kj} V_{\text{H}}[\rho_j](\mathbf{r}). \quad (25)$$

Note that $\delta\rho_{\text{fit}}[\rho](\mathbf{s})/\delta\rho(\mathbf{r})$ does not depend on the charge density ρ because the constrained charge fitting procedure outlined above is a linear operation. Using this general expressing, the variationally consistent Coulomb potential, Eq. (23), becomes

$$\tilde{V}_{\text{H}}[\rho](\mathbf{r}) = V_{\text{H}}[\rho_{\text{fit}}](\mathbf{r}) + \sum_{kj} [\rho - \rho_{\text{fit}}|\rho_k\rangle G_{kj} V_{\text{H}}[\rho_j](\mathbf{r}). \quad (26)$$

Because we determined the fitted charge density with a variational strategy, Eq. (6), the second term cancels, more precisely, $\sum_k [\rho - \rho_{\text{fit}}|\rho_k\rangle G_{kj} = 0$. Therefore, the variationally consistent Hartree potential finally reduces to

$$\tilde{V}_{\text{H}}[\rho] = V_{\text{H}}[\rho_{\text{fit}}]. \quad (27)$$

The apparent simplicity of this result should not be mistaken. It is not a general feature of the variational consistency concept but rather a consequence of the particular energy expression (22) in combination with variational fitting. Any other approximation to $\tilde{E}_{\text{H}}[\rho]$ would result in a noticeably more complicated expression for $\tilde{V}_{\text{H}}[\rho](\mathbf{r})$, for example, as given below for the xc potential.

In a similar way, one obtains the partial derivative $\partial\tilde{E}_{\text{H}}/\partial\lambda$ of the approximate Hartree energy, which enters the first-order total energy derivative, Eq. (3):

$$\frac{\partial\tilde{E}_{\text{H}}}{\partial\lambda} = \left[\rho - \rho_{\text{fit}} \left[\sum_k a_n \frac{d\rho_k}{d\lambda} \right] \right]. \quad (28)$$

This term solely arises from the incompleteness of the charge fit functions with respect to λ derivatives. Again, the simplicity of this formula is exclusively due to the choice of the approximation $\tilde{E}_{\text{H}}[\rho]$ in combination with variational fitting.

EXCHANGE-CORRELATION POTENTIAL IN MDA

The central concept of the MDA is to extend the variationally consistent treatment of the Hartree energy to the xc energy contribution. The approximate xc energy used for that purpose in the MDA approach is a given (nonapproximated) xc energy functional evaluated for the fitted charge density,

$$\tilde{E}_{\text{xc}}[\rho] = E_{\text{xc}}[\rho_{\text{fit}}[\rho]]. \quad (29)$$

The variationally consistent xc potential is then given by the functional derivative of that energy expression with respect to the exact charge density,

$$\tilde{V}_{\text{xc}}[\rho](\mathbf{r}) = \frac{\delta E_{\text{xc}}[\rho_{\text{fit}}]}{\delta \rho(\mathbf{r})}, \quad (30)$$

$$= \int V_{\text{xc}}[\rho_{\text{fit}}](\mathbf{s}) \frac{\delta \rho_{\text{fit}}(\mathbf{s})}{\delta \rho(\mathbf{r})} d^3\mathbf{s}, \quad (31)$$

with $V_{\text{xc}}[\rho](r) = \delta E_{\text{xc}}[\rho]/\delta \rho(r)$ being the original nonapproximated xc potential. As for the Hartree potential, the key quantity for further evaluation of the variationally consistent potential is the partial derivative of the fitted charge density with respect to the exact density. Hence, using Eq. (25), one immediately arrives at

$$\tilde{V}_{\text{xc}}[\rho](\mathbf{r}) = \sum_{kj} \langle V_{\text{xc}}[\rho_{\text{fit}}] | \rho_k \rangle G_{kj} V_{\text{H}}[\rho_j](\mathbf{r}). \quad (32)$$

Apparently, the ultimate, variationally consistent approximation to the xc potential is a linear combination of Coulomb-type terms that at first glance may come as a surprise. This functional dependence arises from the circumstance that the density dependence of the approximate xc functional \tilde{E}_{xc} is exclusively mediated through the fitted charge density and that this fitted charge density is determined by minimizing the Coulomb self-interaction functional, Eq. (6). This introduces a nonlocal Hartree-like response of ρ_{fit} to any change in ρ , as indicated by the functional derivative Eq. (25); we again refer to this point below.

Equation (32) is a special case of the generic first-order derivative of the xc energy, $d\tilde{E}_{\text{xc}}/d\lambda$, which can be obtained by using the λ derivative, Eq. (21), of ρ_{fit} rather than Eq. (25); in other words, here we skip the substitution $\lambda \rightarrow \rho(\mathbf{r})$. Doing so, and leaving out the contribution $d\rho/d\lambda$ associated

with the self-consistent charge density, one obtains the partial derivative of the xc energy needed for the first-order total energy derivative, Eq. (3),

$$\begin{aligned} \frac{\partial \tilde{E}_{\text{xc}}}{\partial \lambda} &= \sum_{kj} \langle V_{\text{xc}}[\rho_{\text{fit}}] | \rho_k \rangle G_{kj} \left[\frac{d\rho_j}{d\lambda} \right] \left[\rho - \rho_{\text{fit}} \right] \\ &+ \sum_{kj} \left\langle V_{\text{xc}}[\rho_{\text{fit}}] \left| \left[1 - \sum_{kj} |\rho_k \rangle G_{kj} [\rho_j] \right] \right. \right| \sum_n a_n \frac{d\rho_n}{d\lambda} \right]. \quad (33) \end{aligned}$$

As in the case of the Hartree energy, the contributions of the xc energy to the total energy derivatives consist of corrections due only to the incompleteness of the charge fit functions with respect to λ derivatives.

The last two expressions, Eqs. (32) and (33), play a central role in the MDA approach. They offer a number of computational advantages over the conventional methodology, which is based on the exact charge density and a fully numerical integration of all xc contributions. First of all, the xc potential, Eq. (32), is expressed in terms of Coulomb-type contributions $V_{\text{H}}[\rho_j]$. This allows one to replace the computationally demanding numerical evaluation of the matrix elements $\langle \chi_\nu | V_{\text{xc}} | \chi_\mu \rangle$ by an analytical evaluation which takes recourse to matrix elements that have already been precalculated. In fact, Eq. (32) can be used to define a combined two-electron fitting coefficient

$$a_k^{\text{ee}} = a_k + \sum_j \langle V_{\text{xc}}[\rho_{\text{fit}}] | \rho_j \rangle G_{jkr} \quad (34)$$

such that the combined Hartree and xc potential becomes

$$\tilde{V}_{\text{ee}}[\rho](\mathbf{r}) = \sum_k a_k^{\text{ee}} V_{\text{H}}[\rho_k](\mathbf{r}). \quad (35)$$

Hence, the matrix elements of the Hartree and xc potentials can be evaluated simultaneously:

$$\langle \chi_\nu | \tilde{V}_{\text{ee}}[\rho] | \chi_\mu \rangle = \sum_k a_k^{\text{ee}} [\chi_\nu \chi_\mu | \rho_k]. \quad (36)$$

The only extra cost is the solution of a system of linear equations to obtain the xc contribution to the two-electron fitting coefficients a_k^{ee} , Eq. (34). As another convenience of the last few expressions, we note that only relatively little effort is required to incorporate the MDA into an existing KS implementation that already uses the charge density fit-

ting procedure outlined above [16]. A further advantage of MDA is that only the fitted charge density, rather than the exact charge density, has to be evaluated on the numerical integration grid to determine the intermediate projections $\langle V_{xc}[\rho_{\text{fit}}]|\rho_k\rangle$ that enter Eq. (32); the exact charge density ρ is required for the matrix elements $\langle \chi_\nu|V_{xc}|\chi_\mu\rangle$ of the conventional approach.

In detail, in MDA one has to evaluate the charge fit functions on the numerical grid; this operation scales as $N_{\text{fit}}N_{\text{grid}}$, where N_{fit} is the number of charge fit functions and N_{grid} is the number of grid points. On the other hand, in the conventional approach one has to evaluate the orbital basis functions on the numerical grid that scales as $N_{\text{bas}}N_{\text{grid}}$ where N_{bas} is the number of orbital basis functions. In addition, in the conventional approach, the KS orbitals and the density have to be evaluated on the grid that formally is an $O(N^3)$ step, scaling as $(N_{\text{bas}} + 1)N_{\text{occ}}N_{\text{grid}}$, where N_{occ} is the number of occupied KS orbitals; furthermore, the matrix elements $\langle \chi_\nu|V_{xc}|\chi_\mu\rangle$ have to be assembled, which is another $O(N^3)$ step, formally scaling as $N_{\text{bas}}^2N_{\text{grid}}$. The corresponding tasks in the MDA comprise evaluation of the fitted charge density on the grid ($\sim N_{\text{fit}}N_{\text{grid}}$), assembly of the intermediate projections ($\sim N_{\text{fit}}N_{\text{grid}}$) and determination of the xc contributions to a_k^{ee} ($\sim N_{\text{fit}}^2$), which are all $O(N^2)$ steps only.

One can also expect that the accumulation of numerical errors due to the finite integration grid is significantly reduced in the MDA because far fewer quantities are evaluated numerically compared with the conventional approach. Even more importantly, the integrands in the intermediate projections $\langle V_{xc}[\rho_{\text{fit}}]|\rho_k\rangle$ of MDA exhibit noticeably fewer sign changes than do the integrands of the matrix elements $\langle \chi_\nu|V_{xc}|\chi_\mu\rangle$ of the conventional approach.

Nevertheless, despite the very useful properties of expression (32), numerical problems, related to the quality of charge density fit, Eq. (5), may arise. Apparently, the Hartree contributions $V_{\text{H}}[\rho_j]$ entering Eq. (32) play the role of basis functions for a variationally consistent representation $\tilde{V}_{xc}[\rho]$ of the xc potential, but their asymptotic behavior is quite different from that of the exact xc potential [55, 56]. Therefore, one anticipates that a more flexible fitting basis $\{\rho_k\}$ is required to satisfy the additional requirements imposed by Eq. (32). The auxiliary (fitting) basis set of a conventional approach is usually quite sufficient for an accurate representation of the electron distribution of a molecular system (up to a limited number of multipole moments) and the resulting Hartree potential [17]. However, this

charge fitting basis may provide only a relatively poor description of the xc potential in MDA. In the next section, devoted to an evaluation of the performance of MDA, we address precisely this question, and we discuss strategies for extending a conventional charge fitting basis set.

Another numerical problem arises from the fact that the fitted charge density ρ_{fit} may exhibit (small) negative values in the low-density regime; in the Appendix, we discuss strategies to cope with this issue.

Fitting Basis Sets for MDA and Benchmark Applications

To construct the auxiliary basis set for MDA calculations, some precaution is necessary, as already mentioned. It is natural to start with a conventional fitting basis set, but it is also of interest if and how one can achieve an accuracy with MDA calculations that compares to that of standard conventional calculations where the xc terms are evaluated via numerical integration. In the following, we first examine the performance of various extensions of the auxiliary basis set, using a set of small main-group molecules. Having established a procedure to construct a reliable fitting basis for MDA calculations, we explore how this scheme performs for diatomics, polyatomic molecules, and transition-metal carbonyls as prototype metal complexes. We conclude this section with example calculations, including large metal clusters, that illustrate the computational efficiency achievable with the MDA strategy.

AUGMENTING THE CHARGE FITTING BASIS SET

To explore possible extensions of the fitting basis set required for MDA calculations, we performed LDA and GGA (Becke–Perdew [BP] [57, 58]) calculations on a set of 37 representative molecules, taken at experimental geometry: Cl₂, F₂, H₂, Li₂, N₂, Na₂, O₂, P₂, S₂, CH, CO, ClO, LiH, HF, OH, NO, SiO, CN, HCl, FCl, LiF, NH, NaCl, SC, CH₂, CO₂, NH₂, H₂O, PH₂, SH₂, SO₂, SiH₂, C₂H₂, C₂H₄, CH₄, HCN, and NH₃, as well as on the atoms constituting these molecules. In these calculations, we used two types of Gaussian-type orbital (GTO) basis sets, to be referred to as I [59] and II [60, 61]; their compositions and the corresponding generalized contraction schemes are summarized in Table I. The

TABLE I
Uncontracted and contracted molecular orbital basis sets.

	I ^a		II ^b	
	Exponents	Contr ^c	Exponents	Contr ^c
H	(6s1p)	[4s1p]	(8s4s3d)	[4s3p2d]
Li	(9s4p)	[4s2p]	(14s9p4d3f)	[4s3p2d1f]
C	(9s5p1d)	[7s4p1d]	(14s9p4d3f)	[5s4p3d2f]
N	(9s5p1d)	[5s4p1d]	(14s9p4d3f)	[7s7p4d3f]
O	(9s5p1d)	[5s4p1d]	(14s9p4d3f)	[5s4p3d2f]
F	(9s5p1d)	[5s4p1d]	(14s9p4d3f)	[7s7p4d3f]
Na	(12s8p2d)	[6s5p2d]	(17s12p5d4f)	[7s7p5d4f]
Si	(12s9p2d)	[6s4p2d]	(17s12p5d4f)	[7s7p5d4f]
P	(12s9p2d)	[6s5p2d]	(17s12p5d4f)	[7s7p5d4f]
S	(12s9p2d)	[6s5p2d]	(17s12p5d4f)	[7s7p5d4f]
Cl	(12s9p1d)	[9s6p1d]	(17s12p5d4f)	[7s7p5d4f]
Fe	(15s11p6d)	[6s5p3d]	(21s15p10d6f4g)	[6s5p4d3f2g]
Ni	(15s11p6d)	[7s6p3d]	(21s15p10d6f4g)	[8s7p6d5f4g]
Au	(19s15p10d6f)	[11s10p7d3f]	—	—

^a For H to Cl, Ref. [59]; Fe, Ref. [69]; Ni, Ref. [70]; Au, Ref. [72].

^b Refs. [60], [61].

^c Generalized contractions using atomic KS eigenvectors of LDA calculations.

fitting basis sets related to these orbital basis sets are denoted as I_n and II_n.

Fitting basis sets I₀ and II₀ are constructed according to a standard procedure [16, 62] employed in the code PARAGAUSS [46]. These basis sets consist of *s*- and *r*²-type Gaussian-type functions, whose exponents are obtained by scaling the exponents of the corresponding orbital basis *s*- and *p*-type primitives, respectively, by a factor of two. The standard fitting bases also include functions that are not spherically symmetric with respect to their atomic centers, namely 5 *p*- and 5 *d*-type “polarization” functions with exponents chosen as geometrical series: (0.1) × 2.5^μ and (0.2) × 2.5^μ (μ = 0 ⋯ 4), respectively [16].

These standard fitting bases were augmented by various *s*-type GTOs and polarization exponents of higher angular momentum GTOs, normally of *f*-type; for H and Li, polarization exponents of basis I were of *d*-type. (Basis I₄ forms a special case; see below.) The exponents for the *s*-type functions were obtained by scaling the smallest *s*-type exponent of the fitting basis (SEFB). The exponents of higher angular momentum fitting functions were selected from geometrical series: (0.3) × 2.5^ν (ν = 0 ⋯ 4) for *f*-type functions and (0.2) × 2.5^ν for *d*-functions (values in a.u.). For brevity, we refer to these additional polarization functions as *f*_ν and *d*_ν, respectively. Basis set II₀ contained *d*-type fitting functions

also for H and Li; therefore, only *f*-type exponents were added in the augmentation process. Altogether, we examined the following 15 fitting basis sets to determine how sensitive MDA results are to various components of the fitting basis set: I₀, standard fitting basis set; I₁, I₀ + 1 *s* exponent (1/3 *s*-SEFB = *s* exponent at 1/3 of SEFB); I₂, I₀ + 2 *s* exponents (1/3 and 1/9 *s*-SEFB); I₃, I₀ + 2 *s* exponents (1/4 and 1/9 *s*-SEFB); I₄, I₁ + 1 *d* exponent (1/2.5 *d*-SEFB, *p*-SEFB for H and Li); I₅, I₁ + *f*_ν *d*_ν polarization exponents, ν = 0 (*d*-type for H and Li); I₆, I₁ + *f*_ν *d*_ν polarization exponents, ν = 1; I₇, I₁ + *f*_ν *d*_ν polarization exponents, ν = 0, 1; I₈, I₁ + *f*_ν *d*_ν polarization exponents, ν = 1, 2; I₉, I₁ + *f*_ν *d*_ν polarization exponents, ν = 0 ⋯ 2; I₁₀, I₁ + *f*_ν *d*_ν polarization exponents, ν = 0 ⋯ 4; II₀, standard fitting basis set; II₁, II₀ + 1 *s* exponent (1/3 *s*-SEFB); II₅, II₁ + *f*_ν polarization exponents, ν = 0; and II₉, II₁ + *f*_ν polarization exponents, ν = 0 ⋯ 2.

In Table II, for each of these fitting basis sets, we compared LDA total energies calculated by MDA to those obtained with the conventional approach based on full numerical (NUM) integration of the xc contributions (MDA vs. NUM). On average, MDA total energies ⟨|ΔE_{tot}⟩ deviate 0.73 kcal/mol from those of the conventional approach (NUM) for basis sets I and 0.63 kcal/mol for basis II; the corresponding maximum deviations |ΔE_{tot}^{max} are 2.85 and 3.26 kcal/mol, respectively.

TABLE II

Comparison of LDA total energies (kcal/mol) of MDA, NUM, and NUM with the standard fitting basis set I₀ or II₀ (NUM/X₀), at experimental geometries.^a

Basis set	MDA vs. NUM			NUM vs. NUM/X ₀ ^b		
	$\langle \Delta E_{\text{tot}} \rangle$	$ \Delta E_{\text{tot}} ^{\text{max}}$		$\langle \Delta E_{\text{tot}} \rangle$	$ \Delta E_{\text{tot}} ^{\text{max}}$	
I ₀	0.73	2.85	Si	—	—	—
I ₁	0.50	1.42	SO ₂	0.00	-0.06	Si
I ₂	1.05	3.29	Cl ₂	0.04	-0.15	Cl ₂
I ₃	0.57	1.88	Cl ₂	0.00	-0.06	Si
I ₄	0.69	2.49	Cl ₂	0.00	-0.06	Si
I ₅	0.61	1.63	C ₂ H ₄	0.15	1.00	Si ₂
I ₆	0.29	-0.65	Cl ₂	0.22	-0.65	Cl ₂
I ₇	0.29	0.67	H ₂ O	0.22	-0.65	Cl ₂
I ₈	0.20	-0.65	Cl ₂	0.25	-0.67	C ₂ H ₄
I ₉	0.17	-0.54	Cl	0.25	-0.67	C ₂ H ₄
I ₁₀	0.17	-0.54	Cl	0.25	-0.68	C ₂ H ₄
II ₀	0.63	3.06	Cl ₂	—	—	—
II ₁	0.67	3.26	Cl ₂	0.00	0.0	—
II ₅	0.16	0.50	C ₂ H ₄	0.24	-0.96	Cl ₂
II ₉	0.07	0.27	Si ₂	0.26	-0.96	Cl ₂

^a Shown are the mean deviation $\langle|\Delta E_{\text{tot}}|\rangle$ over all test systems (see text), the system for which the maximum (absolute) deviation $|\Delta E_{\text{tot}}|^{\text{max}}$ occurs and the corresponding (signed) deviation.

^b Basis set I or II.

Comparing with the MDA results for basis sets I₁–I₃ (Table II), one notes that one additional *s*-type GTO in I₁ improves the accuracy, but further variations do not do so in any appreciable way. Also, augmenting the fitting basis set with polarization functions of low angular momentum (basis I₄) does not amend the MDA results beyond those of I₁. On the other hand, comparing the numerical results among each other (NUM vs. NUM/I₀), that is, the results obtained with augmented fitting basis sets I₁–I₄ to those of the standard basis set I₀, one notes that the scaling technique adopted in PARAGAUSS [16, 62] yields well-converged fitting basis sets when restricted to low angular momenta.

The consistency of the MDA and numerical results could be substantially improved by extending the fitting basis sets by diffuse *f*-type functions (basis sets I₅–I₁₀). The mean deviations $\langle|\Delta E_{\text{tot}}|\rangle$ of total energies was reduced to 0.17 kcal/mol (Table II), which is more than four times smaller than for basis set I₀. The maximum deviation $|\Delta E_{\text{tot}}|^{\text{max}}$ drops by a factor of five. It is worth noting that two additional *f_v*, *d_v*-type exponents (basis I₈) seems to provide almost as accurate results as the large basis sets I₉ and I₁₀. Purely numerical results (without MDA) show average deviations $\langle|\Delta E_{\text{tot}}|\rangle$ of up to 0.25 kcal/mol for the most flexible auxiliary basis sets (with

$|\Delta E_{\text{tot}}|^{\text{max}}$ up to about 0.7 kcal/mol); these results again illustrate the quality of the standard basis set I₀.

Essentially the same conclusions were reached for the second MO basis set, and the corresponding fitting basis sets II₀, II₁, II₅, and II₉ (Table II), for comparisons: MDA versus numerical results of the same auxiliary basis set and numerical results relative to the reference II₀. Again, even one exponent of higher angular momentum (basis II₅) yields notably improved MDA results as compared with the reference II₀. The MDA results for the larger basis sets II₅ and in particular II₉ are very satisfactory; average deviations $\langle|\Delta E_{\text{tot}}|\rangle$ are as small as 0.16 and 0.07 kcal/mol, respectively, and the maximum deviations are 0.50 and 0.27 kcal/mol.

In summary, basis functions of higher angular momentum (*f*-type; *d*-type for H and Li) clearly improve the agreement between MDA and numerical results for the same auxiliary basis set. Based on the results of Table II, we aimed at extensions of the standard fitting basis sets of PARAGAUSS [16, 62] that represent a compromise between accuracy and computational effort. Therefore, we decided to use two type of extensions in the remaining evaluation procedure of the MDA: one additional *s*-type function with an exponent one third of the smallest *s*

TABLE III

Mean square deviations $\langle \Delta E_{\text{tot}}^2 \rangle^{1/2}$ (kcal/mol) of total energies between MDA and NUM calculations at the LDA level, averaged over all interatomic distances used, as well as the corresponding deviations $|\Delta l|$ (Å) of equilibrium bond lengths, $|\Delta \omega|$ (cm^{-1}) of harmonic frequencies, and $|\Delta E_{\text{at}}|$ (kcal/mol) of atomization energies for Li_2 and CO and averages over a set of diatomic molecules.

Basis set	Li_2			CO			Average ^a					
	$\langle \Delta E_{\text{tot}}^2 \rangle^{1/2}$	$ \Delta l $	$ \Delta \omega $	$ \Delta E_{\text{at}} $	$\langle \Delta E_{\text{tot}}^2 \rangle^{1/2}$	$ \Delta l $	$ \Delta \omega $	$ \Delta E_{\text{at}} $	$\langle \Delta E_{\text{tot}}^2 \rangle^{1/2}$	$ \Delta l $	$ \Delta \omega $	$ \Delta E_{\text{at}} $
I_0	0.495	0.0102	0.4	0.33	0.248	0.0013	0.1	0.25	0.38	0.0029	6.1	0.31
I_1	0.478	0.0101	4.6	0.39	0.224	0.0010	2.5	0.09	0.39	0.0033	6.4	0.42
$I_{1,100}$	0.069	0.0012	0.6	0.03	0.225	0.0004	1.1	0.14	0.34	0.0024	5.0	0.32
$I_{1,010}$	0.298	0.0023	2.7	0.17	0.047	0.0002	0.3	0.05	0.36	0.0022	4.0	0.18
$I_{1,011}$	0.281	0.0012	2.4	0.15	0.039	0.0002	0.2	0.03	0.25	0.0018	4.5	0.12
$I_{1,110}$	0.055	0.0003	0.3	0.02	0.085	0.0012	2.7	0.01	0.29	0.0019	4.4	0.15
$I_{1,111}$	0.052	0.0002	0.3	0.02	0.087	0.0003	0.0	0.05	0.20	0.0016	4.0	0.11
II_0	0.050	0.0001	1.1	0.03	0.200	0.0002	2.0	0.06	0.44	0.0002	5.2	0.50
II_1	0.053	0.0010	1.0	0.03	0.211	0.0001	2.1	0.07	0.47	0.0007	6.6	0.53
$II_{1,100}$	0.045	0.0002	0.1	0.02	0.214	0.0002	1.7	0.04	0.45	0.0014	7.0	0.48
$II_{1,010}$	0.049	0.0011	0.3	0.02	0.100	0.0002	1.3	0.02	0.13	0.0006	3.4	0.09
$II_{1,011}$	0.050	0.0010	0.2	0.02	0.042	0.0001	0.9	0.12	0.07	0.0003	1.4	0.11
$II_{1,110}$	0.045	0.0003	0.8	0.02	0.131	0.0001	2.4	0.03	0.17	0.0005	1.5	0.16
$II_{1,111}$	0.045	0.0001	0.8	0.02	0.046	0.0001	0.6	0.07	0.07	0.0002	1.5	0.11

^a Average over Li_2 , CO, LiH, LiF, FH, F_2 , Cl_2 , N_2 , Na_2 , and NaCl.

exponent of the standard fitting basis; and up to three polarization exponents of an angular momentum $l_{\text{max}} + 1$ with $\nu = 0 \cdots 2$, where $l_{\text{max}}(X_0)$ is the maximum value of the reference basis ($X = \text{I or II}$).

The designation X is a generic term of a basis set; the largest basis sets used subsequently were of type X_0 . For basis sets I, l_{max} is 1 for H and Li and 2 for all other elements; in the case of basis II, $l_{\text{max}} = 2$ for all elements. We continue to refer to the fitting basis sets, augmented by one s-type function, as I_1 and II_1 , but we change to a binary three-digit notation, referring to $\nu = 0, 1$, or 2, to specify additional fitting exponents of higher angular momentum. For instance, for carbon, basis $I_{1,111} = I_0$ refers to an extension of I_1 by three f-type polarization exponents 0.300, 0.750, and 1.875 a.u. On the other hand, for Li, basis $I_{1,010}$ comprises one additional polarization exponent beyond basis set I_1 , namely, 0.5 a.u. from the d-type series for $\nu = 1$.

DIATOMIC AND POLYATOMIC MOLECULES

To test the performance of the MDA for describing potential energy curves, we first carried out LDA calculations with six different fitting basis sets on a small set of diatomic molecules: Li_2 , CO, LiH, LiF, HF, F_2 , Cl_2 , N_2 , Na_2 , NaCl. For each of these test

molecule and for each of the six possible extensions of the fitting basis set conforming to the choice just described (see Table III), we performed single-point calculations for different bond lengths. Using five-point polynomial fits, we determined equilibrium bond lengths l and harmonic vibrational frequencies ω from these lists of energy values, and we calculated atomization energies E_{at} at optimized distances.

In Table III, we illustrate for Li_2 and CO how these characteristics obtained by MDA differ from those of the conventional numerical approach using the same fitting basis set. We also show mean square deviations $\langle \Delta E_{\text{tot}}^2 \rangle^{1/2}$ of the total energy values over all distances investigated, typically 10–20 points per diatomic around the energy minimum. The criterion $\langle \Delta E_{\text{tot}}^2 \rangle^{1/2}$ clearly demonstrates the improved agreement between MDA and NUM calculations when the reference fitting basis sets I_0 and II_0 are extended as described above. After maximum augmentation to $I_{1,111}$ and $II_{1,111}$, respectively, the deviations are very uniform along the potential energy curve; see Figure 1. The data of Table III corroborate that fitting functions of higher angular momentum play an important role for the accuracy of MDA calculations.

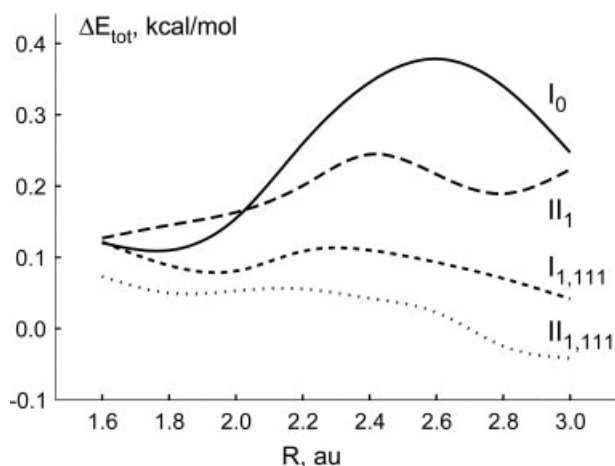


FIGURE 1. Differences ΔE_{tot} of LDA total energies between NUM and MDA calculations for CO as a function of the bond length R for the fitting basis sets I_0 , II_1 , $I_{1,111}$, and $II_{1,111}$.

Detailed inspection of Table III reveals that adding the second and third f -type functions to the standard X_0 or the s -type augmented fitting basis X_1 leads to a substantial reduction of the deviations. For the basis sets $X_{1,111}$, deviations Δl of the bond length are at most 0.0003 \AA , deviations $\Delta\omega$ of the harmonic frequency are less than 1 cm^{-1} , and the atomization energies E_{at} deviate at most 0.07 kcal/mol (Table III). Compared with these results, the basis sets $I_{1,100}$ and $II_{1,100}$ perform relatively poorly.

Apparently, fitting basis sets without the full set of f -type exponents, that is, smaller than $X_{1,111}$, perform differently for the two molecules. To arrive at a more conclusive answer as to which of the five f -type augmented basis sets performs best, we averaged the key quantities over the set of 10 diatomics mentioned above. From the average values, also displayed in Table III, one concludes that the fitting basis sets with f -type exponents for MO basis I all perform rather similarly. However, the performance of fitting basis sets with f -type exponents is uniformly good for both groups of basis sets, I and II, only when the second and third f -type exponents of the three-term series are included.

Therefore, we restricted the subsequent benchmark calculations, which aimed at both LDA and GGA results, to the fitting basis sets $X_{1,011}$ and $X_{1,111}$ which we compared with the corresponding reference results for X_0 ($X = I, II$). In these calculations, we used an enlarged set of diatomic molecules (Table IV).

These results can be summarized as follows. For both groups of fitting basis sets, I and II, extension by s - and f -type exponents leads to improved results for the bond distance, both at the LDA and the GGA level of theory. For the smaller basis set I, MDA calculations reproduce bond distances to $\sim 0.001 \text{ \AA}$ at the LDA level and to $\sim 0.002 \text{ \AA}$ at the GGA level. For the more flexible basis set II, GGA bond distances of MDA calculations agree to $\sim 0.001 \text{ \AA}$ with those of a fully numerical treatment of the xc contributions (NUM). Deviations of harmonic vibrational frequencies in MDA calculations are $5\text{--}8 \text{ cm}^{-1}$ with reference basis sets X_0 . These deviations are only slightly reduced, to 4 and 5 cm^{-1} in LDA and GGA calculations, respectively, when fitting basis set I_0 is augmented to $I_{1,111}$. The MDA calculations with fitting basis sets for MO basis II, for example, $II_{1,111}$, are a bit more accurate, with deviations ~ 2 and 4 cm^{-1} in LDA and GGA calculations, respectively. The energy criteria $\langle \Delta E_{\text{tot}}^2 \rangle^{1/2}$ and $|\Delta E_{\text{at}}|$ yield rather comparable values for a given xc approximation and fitting basis set. The effect of augmentation beyond the reference X_0 is important in all cases. The atomization energies of MDA calculations reproduce the numerical results particularly well for the fitting basis $II_{1,111}$, with deviations of ~ 0.1 and $\sim 0.2 \text{ kcal/mol}$ for LDA and GGA, respectively.

All results on diatomics (Table IV) consistently indicate for both groups of basis sets, I and II, and all extensions of the fitting sets that quality of the fitted charge density are better in LDA than in GGA calculations. Essentially all criteria used in Table IV corroborate this statement, but the conclusions are particularly clear for the two energy characteristics.

At this stage it seems worthwhile to compare pertinent quantities of the MDA and the conventional (numerical, NUM) approach in real space. For this purpose, we compare in Figure 2 the exact [Fig. 2(a)] and the fitted charge densities [Figs. 2(b) and 2(c)] for the molecule Cl_2 from LDA calculations as well as the resulting exact xc correlation potential V_{xc} and the variationally consistent counterparts \tilde{V}_{xc} for the fitting basis sets I_0 and $I_{1,111}$.

The negative tails in the fitted charge density (panel b) are clearly discernible along the molecular axis at the sides opposite of the molecular bond. Note that the special negative contour values adopted in Figure 2 emphasize the low-density regime. By switching to extended fitting basis $I_{1,111}$ (panel c) the negative tails in the fitted charge density are suppressed to a large extent.

TABLE IV

Mean square deviations $\langle \Delta E_{\text{tot}}^2 \rangle^{1/2}$ of total energies (averaged over all interatomic distances used, for diatomics), total energy differences $\langle \Delta E_{\text{min}} \rangle$ at the optimized geometry (for polyatomics) between MDA and NUM calculations at the LDA and GGA levels, as well as the corresponding deviations Δl (Å) of equilibrium bond lengths, $\Delta \varphi$ (degrees) of equilibrium bond angles, $\Delta \omega$ (cm^{-1}) of harmonic frequencies, and $|\Delta E_{\text{at}}|$ of atomization energies (energies in kcal/mol).

Basis set	Diatomics ^a				Polyatomics ^b				
	$\langle \Delta E_{\text{tot}}^2 \rangle^{1/2}$	$\langle \Delta l \rangle$	$\langle \Delta \omega \rangle$	$\langle \Delta E_{\text{at}} \rangle$	$\langle \Delta E_{\text{min}} \rangle$	$\langle \Delta l \rangle$	$\langle \Delta \varphi \rangle$	$\langle \Delta \omega \rangle$	$\langle \Delta E_{\text{at}} \rangle$
LDA									
I ₀	0.35	0.0018	5.2	0.38	0.68	0.0013	0.12	8.8	0.87
I _{1,011}	0.20	0.0013	3.9	0.09	0.07	0.0004	0.06	5.2	0.05
I _{1,111}	0.17	0.0012	3.9	0.14	0.08	0.0003	0.05	5.5	0.05
II ₀	0.43	0.0007	5.6	0.42	0.32	0.0003	0.09	7.7	0.32
II _{1,011}	0.08	0.0001	1.6	0.11	0.03	0.0003	0.02	2.5	0.06
II _{1,111}	0.07	0.0003	1.6	0.08	0.04	0.0002	0.02	2.5	0.06
GGA									
I ₀	0.91	0.0027	5.8	0.52	1.37	0.0011	0.24	16	1.39
I _{1,011}	0.38	0.0017	4.9	0.27	0.29	0.0002	0.07	6.4	0.24
I _{1,111}	0.39	0.0017	4.9	0.25	0.31	0.0001	0.04	11	0.19
II ₀	0.88	0.0013	8.1	0.73	0.78	0.0013	0.17	17	0.69
II _{1,011}	0.26	0.0009	3.1	0.25	0.11	0.0002	0.04	5.0	0.20
II _{1,111}	0.20	0.0011	4.0	0.22	0.14	0.0001	0.05	5.0	0.19

^a Average over Li₂, CO, LiH, LiF, FH, F₂, Cl₂, N₂, Na₂, NaCl (Table III) plus H₂, O₂, P₂, S₂, CH, NO, OH, CN, ClO, SiO, HCl, FCl, NH, and SC.

^b Average over C₂H₂, C₂H₄, CH₂, CH₄, CO₂, HCN, NH₂, NH, H₂O, PH₂, SH₂, SO₂, and SiH₂.

The artifacts introduced by the negative values of the fitted charge density are substantial when one evaluates the approximate xc potential $\tilde{V}_{\text{xc}}[\rho_{\text{fit}}](r)$ which, according to Eq. (32), is a linear combination of Coulomb-type functions $V_{\text{H}}[\rho_j](r)$. As seen in Figure 2(e) and 2(f), the variationally consistent xc potential, using in MDA with basis set I₀, exhibits quite substantial negative tails on the molecular axis of Cl₂. These artifacts again are much notably reduced for the larger fitting basis set I_{1,111}, leading to an overall good MDA performance.

Although the quality of the charge fit is sufficient to represent properly the Coulomb potential, Coulomb-like terms $V_{\text{H}}[\rho_j]$ of the MDA xc representation $\tilde{V}_{\text{xc}}[\rho_{\text{fit}}]$ have to interfere properly to represent the xc potential, which exhibits a much shorter range, as can typically be illustrated by the dominating $\rho^{1/3}$ term of LDA, which is present in almost all xc functionals. Both effects, the accuracy of the approximate density ρ_{fit} and the proper representation of $V_{\text{xc}}[\rho]$ by $\tilde{V}_{\text{xc}}[\rho_{\text{fit}}]$ are compounded in MDA. As the results of Table IV show, MDA, when combined with a moderately extended fitting basis set, affords a reasonable accuracy for typical molecular properties. More detailed studies may be nec-

essary to evaluate how well potential energy surfaces of molecular systems are represented at intermediate to large interatomic distances.

Finally, in Table IV, we compare MDA results for a set of 13 polyatomic molecules (C₂H₂, C₂H₄, CH₂, CH₄, CO₂, HCN, NH₂, NH, H₂O, PH₂, SH₂, SO₂, and SiH₂) with results for conventional numerical calculations using the same three types of fitting bases as probed for diatomics, X₀, X₁, and X_{1,111} for X = I, II. Table IV collects deviations of bond lengths, bond angles, vibrational frequencies, atomization energies, and total energies at equilibrium geometry ($\langle |\Delta E_{\text{min}}| \rangle$), all averaged over this set of molecules. Vibrational frequencies were obtained by diagonalizing the Hessian matrix, which was assembled via finite differences of analytical Cartesian gradients, transformed to internal coordinates.

The MDA results for these polyatomic molecules reproduce the numerical calculations with the same accuracy as found above for diatomics. The reference fitting basis sets I₀ and II₀ yield very satisfactory results for structures, in both LDA and GGA calculations. Deviations of bond lengths are at most ~ 0.001 Å, and deviations of bond angles are less than 0.03 degrees. For extended basis sets, MDA

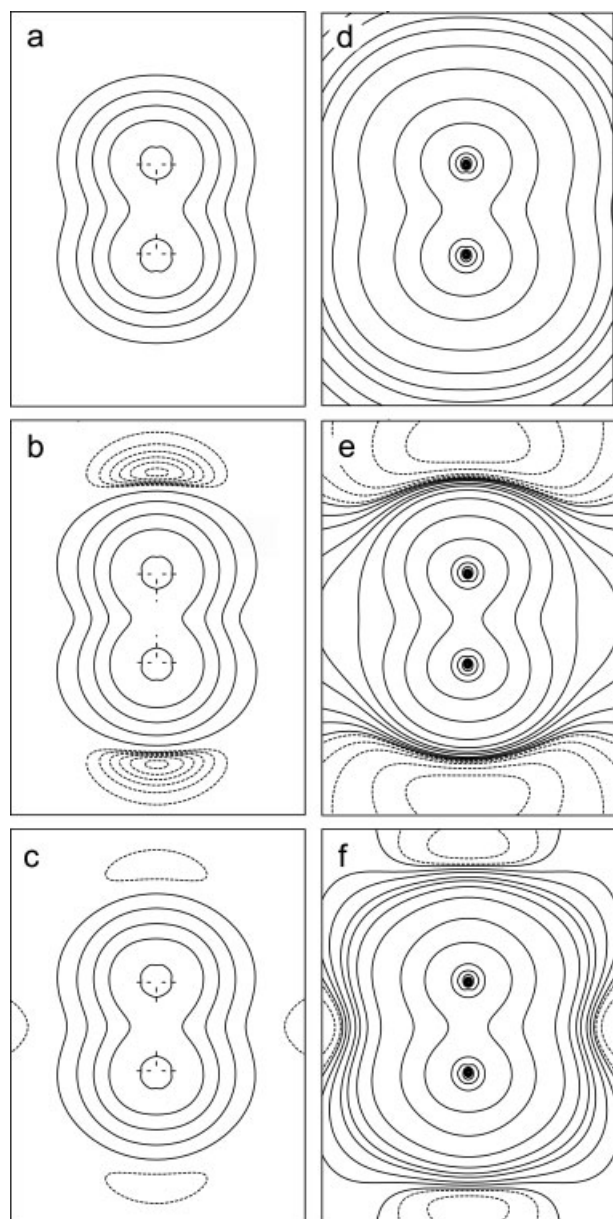


FIGURE 2. Comparison of densities and xc potentials for a Cl_2 molecule from LDA calculations: (a) exact electron density ρ , approximate densities ρ_{fit} for (b) the reference fitting basis set I_0 and (c) the maximally extended basis set $I_{1,111}$, (d) exact xc potential V_{xc} and resulting MDA xc potentials \tilde{V}_{xc} , (e) for I_0 and (f) for $I_{1,111}$. The contour values for panels (a)–(c) are 1.0, 0.2, 0.08, 0.005, 0.001, -0.00001 , -0.0001 , -0.0002 , -0.0003 , -0.0004 , -0.0005 a.u., and those for panels (d)–(f) are 6.0, 5.5, 5.0, 4.5, 4.0, 3.0, 2.0, 1.0, 0.5, 0.25, 0.1, 0.05, 0.03, 0.02, 0.01, 0.005, 0.001, -0.001 , -0.005 , -0.01 , -0.02 , -0.03 a.u.

results for this set of test molecules reproduced the numerical results essentially quantitatively. Also, MDA values of vibrational frequencies and, in par-

ticular, energetics clearly demonstrate the positive effect of extended fitting basis sets. With basis sets $I_{1,111}$ and $II_{1,111}$, atomization energies of numerical calculations are reproduced by MDA to ~ 0.05 kcal/mol for LDA and ~ 0.2 kcal/mol for GGA (Table IV). Different from the tests for diatomics, both MO basis sets I and II, together with their corresponding extended fitting bases, perform about equally well. Yet, as found above, the MDA results for GGA calculations deviate somewhat more from the corresponding numerical calculations than the results of LDA calculations.

TRANSITION METAL CARBONYLS

From the results of the above benchmark calculations one can conclude that standard fitting bases, used routinely in DF calculations with PARAGAUSS [16, 62], perform very satisfactory in MDA calculations when extended by one s -type and three f -type exponents. In the following, we finally test this prescription for constructing auxiliary basis sets for transition metal systems, using two carbonyl complexes as examples.

Transition-metal carbonyl complexes play an important role in organometallic chemistry; they have been intensively studied theoretically [63–68]. For the current purpose, we selected $\text{Ni}(\text{CO})_4$ and $\text{Fe}(\text{CO})_5$. We carried out LDA (Vosko–Wilk–Nusair) and GGA (BP) calculations, using again two types of MO basis sets (Table I) [59–61, 69, 70]. In line with the above conclusions, we extended the standard fitting basis sets following the prescription $X_{1,111}$ (see Table I). We optimized the structure imposing T_d symmetry for $\text{Ni}(\text{CO})_4$ and D_{3h} symmetry for $\text{Fe}(\text{CO})_5$ (Table V). We also calculated the harmonic vibrational frequencies compatible with these constraints (Table VI). In addition to the structure deviations, we monitored the total energy difference ΔE_{tot} (Table V) and the first carbonyl dissociation energies (Table VII). The latter quantities were calculated as total energy differences between two optimized structures for each system, that is, implying the final states $\text{Ni}(\text{CO})_3$ (D_{3h}) and $\text{Fe}(\text{CO})_4$ (C_{2v}) [64, 68]; for $\text{Fe}(\text{CO})_4$ we took two states into account: 1A_1 and 3B_1 .

At the LDA level, MDA calculations with extended fitting basis sets $X_{1,111}$ reproduce bond lengths to 0.001 Å or better (Table V). At the GGA level, MDA results, in particular for metal–carbon bonds, can deviate up to 0.002 Å; however, the axial Fe–C bonds are calculated to short by 0.01 Å. The MDA calculations with the extended fitting basis

TABLE V

Deviations^a of total energies and bond lengths at equilibrium geometry between MDA and NUM on Ni(CO)₄ and Fe(CO)₅ (distances in Å, energies in kcal/mol).

Basis set	Ni(CO) ₄			Fe(CO) ₅				
	ΔE_{tot}	$\Delta(\text{Ni}-\text{C})$	$\Delta(\text{C}-\text{O})$	ΔE_{tot}	$\Delta(\text{Fe}-\text{C}_{\text{ax}})$	$\Delta(\text{Fe}-\text{C}_{\text{eq}})$	$\Delta(\text{C}-\text{O}_{\text{ax}})$	$\Delta(\text{C}-\text{O}_{\text{eq}})$
LDA								
I ₀	0.25	-0.0011	0.0004	1.50	-0.0043	-0.0019	0.0003	0.0004
I _{1,111}	-0.21	0.0004	-0.0005	1.67	-0.0042	-0.0013	-0.0002	0.0006
II ₀	-1.49	0.0002	0.0003	-0.87	0.0024	-0.0022	0.0007	0.0003
II _{1,111}	0.04	0.0000	0.0002	1.08	0.0026	-0.0004	0.0001	-0.0002
GGA								
I ₀	-0.47	0.0033	-0.0006	1.41	-0.0078	-0.0038	0.0004	0.0001
I _{1,111}	-1.24	0.0024	-0.0002	1.72	-0.0117	-0.0016	0.0015	-0.0002
II ₀	-2.80	0.0021	0.0004	-4.44	0.0233	0.0113	-0.0019	-0.0006
II _{1,111}	-0.94	-0.0011	0.0006	1.60	-0.0077	0.0007	-0.0005	-0.0003

^a Deviations $\Delta = X(\text{MDA}) - X(\text{NUM})$.

sets are able to reproduce total energies to 2 kcal/mol or better. More flexible MO basis sets (II vs. I) lead to smaller deviations; similar to the above findings, MDA deviations for energies are larger for LDA than for GGA results. Inspection of Table VI shows that vibrational frequencies of KS calculations with numerical treatment of the xc contribu-

tions are very well reproduced in MDA calculations with extended fitting basis sets. Most deviations are below 5 cm⁻¹; only two low-frequency modes of Fe(CO)₅ exhibit deviations of 10 and 7 cm⁻¹ at the GGA level for the fitting basis sets I_{1,111} and II_{1,111}, respectively (Table VI). Even the standard fitting basis sets I₀ and II₀ yield acceptable results for the

TABLE VI

Harmonic frequencies ω of totally symmetry vibrational modes from numerical KS calculations on Ni(CO)₄ and Fe(CO)₅ and the deviations^a $\Delta\omega$ of the corresponding MDA results (all values in cm⁻¹).

Basis	Ni(CO) ₄				Fe(CO) ₅			
	LDA		GGA		LDA		GGA	
	ω	$\Delta\omega$	ω	$\Delta\omega$	ω	$\Delta\omega$	ω	$\Delta\omega$
I ₀	447.1	-6.6	412.8	-1.4	466.8	3.0	429.9	6.4
					490.8	4.2	451.0	8.3
	2156.3	-3.7	2095.2	-1.0	2079.8	-0.6	2017.2	0.0
I _{1,111}	447.1	-4.5	412.9	0.4	2154.5	-0.5	2092.1	0.3
					466.7	2.6	429.6	4.9
	2156.5	-2.8	2095.5	-0.5	491.7	5.0	452.2	9.6
II ₀	442.3	12.4	404.9	16.6	2080.1	0.1	2017.5	0.0
					2154.5	0.3	2091.9	0.3
	2158.9	6.4	2096.9	9.9	467.5	-1.6	429.9	-21.0
II _{1,111}	442.4	-2.2	405.2	1.0	490.4	-1.2	450.1	-18.6
					2083.4	-2.4	2018.8	3.7
	2158.3	-3.8	2096.3	-4.6	2159.5	-2.4	2095.4	3.4
				467.6	0.3	429.8	2.3	
				491.3	2.4	451.5	6.9	
				2083.1	0.4	2018.6	5.0	
				2158.9	0.4	2094.9	5.4	

^a Deviations $\Delta\omega = \omega(\text{MDA}) - \omega(\text{NUM})$.

TABLE VII
First ligand dissociation energies ΔE (kcal/mol) of
Ni(CO)₄ and Fe(CO)₅: $M(\text{CO})_n \rightarrow M(\text{CO})_{n-1} + \text{CO}$.^a

Basis set	Ni(CO) ₃	Fe(CO) ₄ ^b ¹ A ₁	Fe(CO) ₄ ^b ³ B ₁
LDA			
I ₀	-0.59	-0.76	1.20
I ₁₁₁	0.02	-0.58	1.27
II ₀	0.54	-0.54	-0.31
II ₁₁₁	-0.45	-0.65	0.79
GGA			
I ₀	-0.54	-1.16	2.49
I ₁₁₁	0.36	-0.54	1.80
II ₀	0.14	-3.60	-1.67
II ₁₁₁	-0.33	-1.25	-0.46

^a Differences [deviations $\Delta = \Delta E(\text{MDA}) - \Delta E(\text{NUM})$] of reaction energies between MDA and numerical KS calculations.

^b Two states are considered for Fe(CO)₄.

high-frequency modes, with deviations at most 10 cm⁻¹; only some low-frequency modes exhibit larger deviations up to ~20 cm⁻¹.

The first metal–ligand dissociation energy of Ni(CO)₄ is about 25 kcal/mol and that of Fe(CO)₅ is about 40 kcal/mol [64]. Therefore, with deviations of at most 0.5 kcal/mol, MDA calculations on Ni(CO)₄, using extended basis sets, reproduce the corresponding results of numerical KS calculations in very satisfactory fashion (Table VII). The MDA results for Fe(CO)₅ are somewhat less accurate. However, these MDA results are still adequate in view of the experimental binding energies just mentioned, even though the deviations for the state ³B₁ are up to 1.8 kcal/mol.

COMPUTATIONAL EFFICIENCY OF MDA

In this section we return to the ultimate aim of the MDA, the reduction of the computational effort for DFT studies. To measure the efficiency of MDA compared with the conventional approach employing numerical integration (NUM) for the xc contributions, we selected three systems that are of interest to our current research: two large metal clusters, Ni₅₅ and Au₅₅, as well as a cluster modeling an active site in a zeolite framework, comprising 12 Si atoms tetrahedrally coordinated by oxygen centers and embedded in an elastic polarizable environment (EPE) [71], which is represented by about 4000 point charges. Table VIII collects various timings

and speed-up factors as obtained with the program PARAGAUSS [46].

To facilitate the comparison, the number of SCF (self-consistent field) cycles has been fixed to 30, a typical number for such systems. Of primary interest is the timing for those parts of the code that deal with the evaluation of the xc contributions to the total energy and the forces as well as the matrix elements of the xc potential. In an MDA calculation, the latter comprises only the evaluation of the xc contributions to the electronic fitting coefficients a_k^{ee} in Eq. (34), because the final assembling of the matrix elements $\langle \chi_\nu | V_{\text{xc}} | \chi_\mu \rangle$ is done without additional cost, together with the evaluation of the corresponding matrix elements $\langle \chi_\nu | V_{\text{H}} | \chi_\mu \rangle$ of the Hartree potential, using Eq. (36).

In the second section, we discussed in detail the computational effort for the individual computational steps and how they scale with the size of the system. Within the conventional approach, two $O(N^3)$ steps of relatively simple, straightforward linear algebra are required in an SCF iteration; together, they scale with $N_{\text{bas}}(N_{\text{bas}} + N_{\text{occ}})N_{\text{grid}}$. On the other hand, in the MDA, these steps have to be compared to three similarly simple steps of $O(N^2)$, scaling with $N_{\text{fit}}(N_{\text{fit}} + 2N_{\text{grid}})$. The bare evaluation of the xc functional is the same in both approaches. Hence, the expected speed-up of MDA relative to NUM calculations depends on the ratio $N_{\text{bas}}/N_{\text{fit}}$ and on the prefactor of the $O(N^3)$ step inherent to the conventional approach.

As can be seen from Table VIII, the density evaluation in MDA calculations exhibits speed-up factors from about 7 to about 130, depending on the system and the fitting basis sets used. Equally nice speed-up factors, ranging from 80 to over 300, were found for the evaluation of the xc contribution to the Hamiltonian. When calculating the time-consuming xc contributions to the forces, one has to evaluate functions and their derivatives on the integration grid; thus, the speed-up is not quite as large, ranging from ~3 for the zeolite cluster to 11–13 for the two metal clusters. When one wants to maintain a comparable accuracy, one has to use extended fitting basis sets; hence, more integrals have to be precalculated. This offsets in part the advantage gained when handling the xc contributions. However, the examples of Table VIII clearly demonstrate a significant overall speed-up, afforded by the MDA. For the total SCF part, these factors range from 3.5 to 9 and for the whole calculations one can expect a saving of about 50% of the computer time, as suggested by overall speed-up

TABLE VIII

Timings of GGA calculations on three example systems with different symmetry constraints.^a

Method basis set	Zeolite cluster (C ₃) ^b			Ni ₅₅ (O _h) ^c			Au ₅₅ (O _h) ^d	
	NUM	MDA		NUM	MDA		NUM	MDA
	l ₀	l ₀	l _{1,111}	l ₀	l ₀	l _{1,111}	l ₀	l _{1,111}
Analyt. integrals, forces	9125	9510	10616	1275	1271	2400	6570	6562
SCF density	4672	425	685	881	14	29	6756	51
SCF xc Hamiltonian ^e	6160	143	171	725	8	9	4556	14
SCF charge fit, eigensolver	1062	1184	1857	61	82	115	3338	3308
SCF remaining tasks	800	1025	888	244	75	63	815	538
SCF total	12937	3030	3601	1911	218	267	15274	3911
xc forces	4495	1501	1728	3819	229	301	701	62
Total	26834	14041	15945	7005	1718	2968	22545	10535
Speedup NUM/MDA								
SCF		4.3	3.6		8.8	7.2		3.9
xc forces		3.0	2.6		6.7	12.7		11.3
Total		1.9	1.7		4.1	2.4		2.1

^a Comparison of various parts of the KS calculations, including the evaluation of the forces, for conventional calculations with NUM and MDA calculations, using various standard (l₀) and extended (l_{1,111}) fitting basis sets. All timings in CPU seconds for 30 SCF iterations on a Pentium III processor. Also given is the speed-up MDA vs. NUM for various parts of a KS calculation.

^b Cluster Si₁₂O₁₂O₂₄ modeling faujasite, with O* pseudobond pseudopotential centers, embedded in an elastic polarizable environment (EPE) comprising 3900 point charges; for details, see Ref. [71].

^c MO basis set from Ref. [70].

^d MO basis set from Ref. [72]; the standard fitting basis of Au already contains 5 *f*-type exponents.

^e The MDA timings contain the time spent for evaluating the projection integrals, Eq. (32).

factors of 1.7–2.4 with l_{1,111} fitting basis sets (Table VIII).

Conclusions

The density fitting technique (also referred to as “resolution of the identity” approach), which is widely used in DFT calculations on molecular systems, has been extended to treat xc contributions in almost fully analytic fashion. This MDA affords essentially the same accuracy for the main characteristics of molecular systems, that is, structure parameters, total and atomization energies, as well as vibrational frequencies. Tests performed for a representative set of diatomic and polyatomic molecules demonstrated that in most cases the overall accuracy of MDA (compared with conventional calculations relying exclusively on numerical integration for the xc contributions) is about 1–1.5 kcal/mol for energies, 0.001 Å for bond lengths, and up to 10 cm⁻¹ for vibrational frequencies. This holds for both LDA and GGA calculations, although MDA results in LDA calculations are usually somewhat more accurate.

Being formulated variationally, the MDA features displacement gradients that are consistent with the energy expression. Moreover, it allows a systematic improvement of the results by improving the quality of the fitting (auxiliary) basis set to represent the electron density and the xc potential. This feature has been demonstrated for a wide range of examples. Based on those results, we proposed a prescription as to how to augment conventional fitting basis sets to avoid a significant loss in the accuracy of the results.

Any existing DF code, which already uses the DF technique can easily be extended to MDA by introducing a new type of projection integrals [see Eq. (32)], whose implementation is straightforward. In MDA, only a relatively small number of the fitting functions has to be precalculated on the integration grid instead of full set of molecular orbital basis functions. This last feature notably reduces the amount of computer resources required by the calculations. The MDA does not fully eliminate numerical integrations, but the amount of the integrations is proportional to the size of fitting basis only; thus, the approach exhibits linear scaling. The number of remaining numeric integrations is also

greatly reduced compared with the conventional approach, thus reducing the computational work by a factor of up to several hundreds. Both these features render the MDA method a very promising tool for DF calculations on large systems.

Appendix: Truncation Schemes for Fitted Charge Densities

The electron density ρ of matter is a positive quantity, and the evaluation of essentially all xc functionals crucially depends on this property; for instance, the kernel of the Dirac–Slater exchange functional [22], proportional to $\rho^{4/3}$, is not defined for regions where the values of ρ become negative. Unfortunately, there is no simple way to ensure that a linear ansatz for an approximate electron distribution, Eq. (5), remains positive semidefinitely. In fact, in practice, one often encounters weak oscillations of density approximations with small negative values in the low-density regions, that is, far away from the nuclei of a system. The diatomic molecule Cl_2 provides a representative example of such an “oscillating” behavior of the electron density (Fig. 2) where negative tails are observed on the side opposite of the bond. An augmented fitting basis [Fig. 2(c)] considerably improves the shape of the approximate electron density compared with that of standard fitting basis [Fig. 2(b)]. Nevertheless, there are still regions where the approximate density is negative. Therefore, special means must be taken to allow a straightforward evaluation of the density functionals.

The simplest procedure (hard truncation) is to introduce a lower threshold τ and to ensure that the approximate electron density $\tilde{\rho}$ remains above this lower bound; in other words, one works with a “truncated” electron density

$$\tilde{\rho} = S_h(\rho_{\text{fit}}, \tau), \quad (37)$$

where S_h is a “hard” shape function

$$S_h(\rho, \tau) = \max(\rho, \tau). \quad (38)$$

The gradient of the truncated density $\tilde{\rho}$ is not continuous. This drawback of procedure (38) may not cause a large problem in the case of LDA functionals, because in conventional schemes $\tilde{\rho}$ is calculated on a grid and one may regard the calculated values

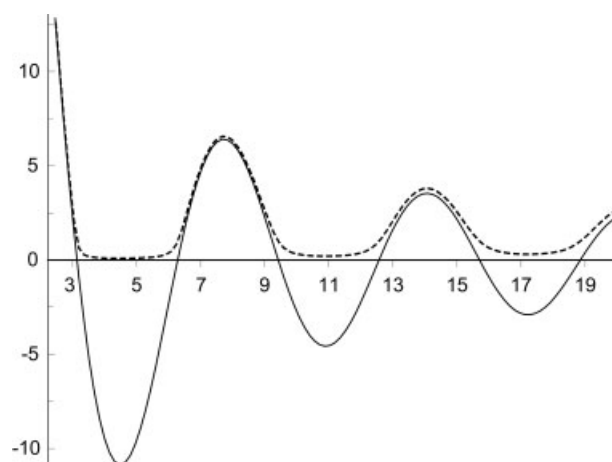


FIGURE 3. Soft truncation $S(x) = S_s(\rho(x), \delta)$ (dashed line) for $\delta = 2$ applied to $\rho(x) = 50 \sin x/x$ (solid line).

of the truncated electron density to represent some smoothed version of $\tilde{\rho}$. However, the accuracy of gradient-corrected functionals may substantially suffer from discontinuities of the density gradient $\nabla\tilde{\rho}$.

Hence, a generalization of the above truncation scheme that guarantees a smooth transition into the threshold regime is required. Conventional broadening techniques are not very convenient in this context because of their intrinsic nonlocal character, which would notably complicate the evaluation of the density functional. Therefore, a local variant of such a smooth truncation is proposed as provided by the following “soft” shape function

$$S_s(\rho, \delta) = [\rho + (\rho^2 + \delta^2)^{1/2}]/2. \quad (39)$$

As above, it leads to a truncated (approximate) density:

$$\tilde{\rho} = S_s(\rho_{\text{fit}}, \delta). \quad (40)$$

The parameter δ controls the smoothness of the transition. Figure 3 demonstrates the effect of the transformation (40) when applied to the function $\rho(x) = 50 \sin x/x$ for the somewhat extreme case $\delta = 2$, to allow displaying the smoothing transition in the figure. For values well above δ , the truncated density $\tilde{\rho}$ very nicely reproduces the given function ρ , but it remains strictly positive.

In a practical implementation, the soft truncation scheme may still yield zero densities, due to the finite precision of machine arithmetics. This hap-

pens for very negative values of the input density, more precisely for $\rho < -\rho_\varepsilon$ where

$$\rho_\varepsilon = \delta(2\varepsilon)^{-1/2}. \quad (41)$$

Here, ε is the smallest positive number for a given machine arithmetics that satisfies the condition $1 + \varepsilon > 1$. For $\rho \rightarrow -\rho_\varepsilon$ the shape function S_s approaches

$$S_s(-\rho_\varepsilon, \delta) \approx \varepsilon\rho_\varepsilon/2 \equiv S_{\varepsilon'} \quad (42)$$

and thus a numerically stable definition of the soft shape function is

$$S_s(\rho, \delta) = \begin{cases} [\rho + (\rho^2 + \delta^2)^{1/2}]/2, & \rho \geq -\rho_\varepsilon \\ S_{\varepsilon'}, & \rho < -\rho_\varepsilon. \end{cases} \quad (43)$$

Some gradient-corrected functionals also may perform rather poorly for small electron densities but still relatively large density gradients. This situation will hardly occur for a normal electron distribution but can arise for a truncated density if the smoothing parameter δ chosen is substantially smaller than $\varepsilon^{1/2}$, which typically is of the order 10^{-7} . In that case, a generalized soft shape function, such as

$$S_e(\rho, \nabla\rho, \delta) = [\rho + (\rho^2 + \delta^2|\nabla\rho|^2)^{1/2}]/2, \quad (44)$$

which dynamically couples the smoothing parameter δ to the local size of the density gradient $\nabla\rho$, will be useful.

To introduce consistently the soft truncation concept into the MDA, one replaces the exact xc energy functional E_{xc} , Eq. (29), by its truncated counterpart

$$E_{xc}^{\text{tr}}[\rho] \equiv E_{xc}[S(\rho)], \quad (45)$$

with $S(\rho)$ as a generic shape function. Then, the corresponding, variationally consistent xc potential that enters Eqs. (30)–(34) is

$$V_{xc}^{\text{tr}}(\mathbf{r}) = \frac{\delta}{\delta\rho(\mathbf{r})} E_{xc}^{\text{tr}}[\rho] = V_{xc}[S(\rho)](\mathbf{r})S'(\rho(\mathbf{r})), \quad (46)$$

where $V_{xc}[\rho] = \delta E_{xc}[\rho]/\delta\rho(\mathbf{r})$ and $S'(\rho)$ is the derivative of the shape function with respect to the input density ρ .

Examples of truncated MDA xc potentials are also presented in Figure 2. Again, augmenting the standard fitting basis by diffuse *s*- and *f*-type fitting

functions (cf. panels e and f of Fig. 2) enhances the overall shape of this approximate xc potential by improving the mutual cancellation in the superposition of various long-range Coulomb-like tails.

ACKNOWLEDGMENTS

This work was supported by Deutsche Forschungsgemeinschaft, Volkswagen Foundation (grant I/73653), INTAS/RFBF (grant IR-97-1071/RFBF 97-03-71057), and Fonds der Chemischen Industrie.

References

- Hohenberg, P.; Kohn, W. *Phys Rev B* 1964, 136, 864.
- Kohn, W.; Sham, L. J. *Phys Rev A* 1965, 140, 1133.
- Koch, W.; Holthausen, M. C. *A Chemist's Guide to Density Functional Theory*; Wiley-VCH: New York, 2000.
- Greeley, J.; Nørskov, J. K.; Mavrikakis, M. *Annu Rev Phys Chem* 2002, 53, 319.
- Perdew, J. P.; Chevary, J. A.; Vosko, S. H.; Jackson, K. A.; Pederson, M. R.; Singh, D. J.; Fiolhais, C. *Phys Rev B* 1992, 46, 6671.
- Perdew, J. P.; Burke, K.; Ernzerhof, M. *Phys Rev Lett* 1996, 77, 3865.
- Hammer, B.; Hansen, L. B.; Nørskov, J. K. *Phys Rev B* 1999, 59, 7413.
- Perdew, J. P.; Kurth, S.; Zupan, A.; Blaha, P. *Phys Rev Lett* 1999, 82, 2544.
- Tao, J.; Perdew, J. P.; Staroverov, V. N.; Scuseria, G. E. *Phys Rev Lett* 2003, 91, 146401.
- Van Voorhis, T.; Scuseria, G. E. *J Chem Phys* 1998, 109, 400.
- Tozer, D. J.; Handy, N. C. *J Chem Phys* 1998, 108, 2545.
- Tozer, D. J.; Handy, N. C. *J Phys Chem A* 1998, 102, 3162.
- Hamprecht, F. A.; Cohen, A. J.; Tozer, D. J.; Handy, N. C. *J Chem Phys* 1998, 109, 6264.
- Boese, A. D.; Doltsinis, N. L.; Handy, N. C.; Sprik, M. *J Chem Phys* 2000, 112, 1670.
- Boese, A. D.; Handy, N. C. *J Chem Phys* 2001, 114, 5497.
- Dunlap, B. I.; Rösch, N. *Adv Quant Chem* 1990, 21, 317.
- Eichkorn, K.; Treutler, O.; Öhm, H.; Häser, M.; Ahlrichs, R. *Chem Phys Lett* 1995, 242, 652.
- Eichkorn, K.; Weigend, F.; Treutler, O.; Ahlrichs, R. *Theor Chem Acc* 1997, 97, 119.
- Weigend, F.; Häser, M.; Patzelt, H.; Ahlrichs, R. *Chem Phys Lett* 1998, 294, 143.
- Friesner, R. A. *Annu Rev Phys Chem* 1991, 42, 341.
- Dunlap, B. I. *Int J Quantum Chem* 1998, 69, 317.
- Slater, J. C. *Quantum Theory of Molecules and Solids, Vol. 4*; McGraw-Hill: New York, 1974.
- Whitten, J. L. *J Chem Phys* 1973, 58, 4496.
- Baerends, E. J.; Ellis, D. E.; Ros, P. *Chem Phys* 1973, 241.

25. Dunlap, B. I.; Connolly, J. W. D.; Sabin, J. R. *J Chem Phys* 1979, 71, 3396.
26. Slater, J. C. *Phys Rev* 1951, 81, 385.
27. Te Velde, G.; Baerends, E. J. *J Comp Phys* 1992, 99, 84.
28. Te Velde, G.; Baerends, E. J. *Phys Rev B* 1991, 44, 7888.
29. Becke, A. D. *J Chem Phys* 1998, 88, 2547.
30. Murray, C. W.; Handy, N. C.; Laming, G. J. *Mol Phys* 1993, 78, 997.
31. Stratmann, R. E.; Scuseria, G. E.; Frisch, M. J. *Chem Phys Lett* 1996, 257, 213.
32. Delley, B. *J Chem Phys* 1990, 92, 508.
33. Krack, M.; Köster, A. M. *J Chem Phys* 1998, 108, 3226.
34. Gill, P. M. W.; Johnson, B. G.; Pople, J. A. *Chem Phys Lett* 1993, 209, 506.
35. Johnson, B. G.; Gill, P. M. W.; Pople, J. A. *Chem Phys Lett* 1994, 220, 377.
36. Sambe, H.; Felton, R. H. *J Chem Phys* 1975, 62, 3, 1122.
37. Dunlap, B. I. *J Phys Chem* 1986, 90, 5524.
38. Dunlap, B. I.; Cook, M. *Int J Quantum Chem* 1986, 29, 767.
39. Cheng, Y. C.; Almlöf, J. *Chem Phys Lett* 1993, 214, 397.
40. Werpetinski, K. S.; Cook, M. *Phys Rev A* 1995, 52, R3397.
41. Werpetinski, K. S.; Cook, M. *J Chem Phys* 1997, 106, 17, 7124.
42. Glaesemann, K. R.; Gordon, M. S. *J Chem Phys* 1998, 108, 24, 9959.
43. Zheng, Y. C.; Almlöf, J. *J Mol Struct THEOCHEM* 1996, 288, 277.
44. Birkenheuer, U. *Habilitationschrift; Technische Universität: München*, 1999.
45. Belling, T.; Grauschopf, T.; Krüger, S.; Mayer, M.; Nörtemann, F.; Staufer, M.; Zenger, M.; Rösch, N. In Bugartz, H.-J.; Durst, F.; Zenger, C., Eds. *High Performance Scientific and Engineering Computing: Lecture Notes in Computational Science and Engineering*; Springer: Heidelberg, 1999, p. 439.
46. Belling, T.; Grauschopf, T.; Krüger, S.; Nörtemann, F.; Staufer, M.; Mayer, M.; Nasluzov, V. A.; Birkenheuer, U.; Hu, A.; Matveev, A. V.; Shor, A. M.; Fuchs-Rohr, M. S. K.; Neyman, K. M.; Ganyushin, D. I.; Kerdcharoen, T.; Woiterski, A.; Gordienko, A. B.; Majumder, S.; Rösch, N. *PARA-GAUSS*, Version 3.0; Technische Universität: München, 2004.
47. Hellmann, H. *Einführung in die Quantenchemie*; Deuticke: Leipzig, 1937.
48. Feynman, R. P. *Phys Rev* 1939, 56, 340.
49. Methfessel, M.; Paxton, A. T. *Phys Rev B* 1989, 40, 3616.
50. De Vita, A.; Gillan, M. J. *J Phys Condens Matter* 1991, 3, 6225.
51. Weinert, M.; Davenport, J. W. *Phys Rev B* 1992, 45, 13709.
52. Pulay, P. *Mol Phys* 1969, 17.
53. Jörg, H.; Rösch, N.; Sabin, J. R.; Dunlap, B. I. *Chem Phys Lett* 1985, 114, 529.
54. Dunlap, B. I.; Connolly, J. W. D.; Sabin, J. R. *J Chem Phys* 1979, 71, 4993.
55. Zunger, A. *Phys Rev B* 1980, 22, 649.
56. Latter, R. *Phys Rev* 1955, 99, 510.
57. Becke, A. D. *Phys Rev A* 1988, 38, 3098.
58. Perdew, J. P. *Phys Rev B* 1986, 33, 8822.
59. Poirier, R.; Kari, R.; Csizmadia, I. G. *Handbook of Gaussian Basis Sets: A Compendium for Ab-Initio Molecular Orbital Calculations*; Elsevier: Amsterdam, 1985.
60. Wildmark, P.-O.; Malmqvist, P.-A.; Roos, B. *Theor Chim Acta* 1990, 77, 291.
61. Pou-Amerigo, R.; Merchán, M.; Nebot-Gil, I.; Wildmark, P.-O.; Roos, B. *Theor Chim Acta* 1995, 92, 149.
62. Dunlap, B. I.; Rösch, N. *J Chim Phys* 1989, 86, 671.
63. Ehlers, A. W.; Frenking, G. *J Am Chem Soc* 1994, 116, 1514.
64. Li, J.; Schreckenbach, G.; Ziegler, T. *J Am Chem Soc* 1995, 117, 486.
65. Berces, A.; Ziegler, T. *J Phys Chem* 1995, 99, 11417.
66. Jonas, V.; Thiel, W. *J Chem Phys* 1995, 102, 8474.
67. Berces, A. *J Phys Chem* 1996, 100, 16538.
68. Matveev, A.; Staufer, M.; Mayer, M.; Rösch, N. *Int J Quantum Chem* 1999, 75, 863.
69. Stener, M.; Albert, K.; Rösch, N. *Inorg Chim Acta* 1999, 286, 30.
70. Matveev, A. V.; Neyman, K. M.; Yudanov, I. V.; Rösch, N. *Surf Sci* 1999, 426, 123.
71. Nasluzov, V. A.; Ivanova, E. A.; Shor, A. M.; Vayssilov, G. N.; Birkenheuer, U.; Rösch, N. *J Phys Chem B* 2003, 107, 22.
72. Häberlen, O. D.; Chung, S.-C.; Stener, M.; Rösch, N. *J Chem Phys* 1997, 106, 5189.